Validity of the static-exchange approximation for inner-shell photoionization of polyatomic molecules

Carlos A. Marante,[1] Loren Greenman,[2] Cynthia S. Trevisan,[3] Thomas N. Rescigno,[1] C. William McCurdy,[4,1] and Robert R. Lucchese[1,*]

[1]*Chemical Sciences Division, Lawrence Berkeley National Laboratory, Berkeley, California 94720, USA*
[2]*Department of Physics, Kansas State University, 116 Cardwell Hall, 1228 N. 17th St., Manhattan, Kansas 66506-2601, USA*
[3]*Department of Sciences and Mathematics, California State University, Maritime Academy, Vallejo, California 94590, USA*
[4]*Department of Chemistry, University of California, Davis, California 95616, USA*

(Received 8 May 2020; revised 26 June 2020; accepted 1 July 2020; published 24 July 2020)

The simple single-channel static-exchange approximation completely ignores correlation between the continuum and molecular ion electrons. In molecular systems with symmetry equivalent atoms, the single-channel approximation can seriously fail in core ionization when using delocalized orbitals to represent the core hole states. We present cross sections and molecular frame photoelectron angular distributions with both localized and delocalized core orbitals in CF_4 F ($1s$) ionization. We show that only a full coupled-channel calculation can recover an accurate description of the physics of inner-shell photoionization when using delocalized orbitals, whereas nearly the same result can be obtained from independent single-channel static-exchange calculations when localized core orbitals are used. A grid-based variational method described here makes such single-channel calculations possible on larger systems without local-exchange approximations. Illustrative calculations on the core ionization of SF_6 are presented to illustrate the power of the grid-based method.

DOI: 10.1103/PhysRevA.102.012815

I. INTRODUCTION

The amplitude for photoionization of an atom or molecule is proportional to the matrix element of the dipole operator between the initial state and a continuum wave function for electron-ion scattering. It has been known for some time that in general the accurate calculation of molecular photoionization cross sections requires a close-coupling treatment of the electron-ion scattering wave function in which the ionization channels producing the ion in different electronic states are coupled [1–3]. In recent decades the development of experimental momentum imaging observations of ion fragments and electrons in coincidence have allowed the measurement of molecular frame photoelectron angular distributions (MFPADs) [4,5], and has provided increasingly strict tests of theoretical predictions. In that context it has been observed that, while a coupled channels treatment is frequently necessary for valence photoionization of molecules, the single-channel static-exchange approximation can provide accurate results for core ionization or inner-shell ionization when the ionized state is not degenerate or nearly degenerate. Using this simpler approximation, which ignores correlation between the continuum and bound electrons, combined experimental and theoretical studies have uncovered "imaging" and "anti-imaging" angular distributions in core and inner-shell ionization [6–9] and explored the consequences of core-hole localization in molecules with symmetry equivalent atoms [10–13].

In earlier studies [8,10] it was found that when the ion channels defined by the removal of a core electron from degenerate orbitals arising from symmetry equivalent atoms, for example, the F $1s$ orbitals in CF_4 [10] or carbon $1s$ in ethane [8], channel coupling changed the MFPADs greatly and was necessary to reproduce the experimental angular distributions. On the other hand, for similar molecules, like 1,1-difluoroethylene [8] where both fluorines are on the same carbon, making the carbon atoms inequivalent, the single-channel static-exchange treatment was entirely sufficient.

In the present study we demonstrate that, in cases with equivalent atoms, the approximation of uncoupling degenerate channels can generally misrepresent the physics of core ionization, strongly affect the integral cross sections, and even break the molecular symmetry expected in the body-frame angular distribution of photoelectrons. Moreover, the results of single-channel calculations depend on which equivalent definition of the degenerate channels is used. The sum of the photoionization cross sections for degenerate channels is not invariant to a unitary transformation of the degenerate orbitals from which the ionization takes place. We will discuss the origin of these effects and also propose a procedure that minimizes channel coupling and allows the treatment of both delocalized and localized core hole formation in photoionization in single-channel calculations. This idea is applicable to large systems where coupled channel photoionization calculations may not be feasible.

We explore these questions here using the complex Kohn variational method, which is well established in the literature [14–17], but which in its previous implementation is limited to smaller systems. To extend that method to larger systems

*Corresponding author: rlucchese@lbl.gov

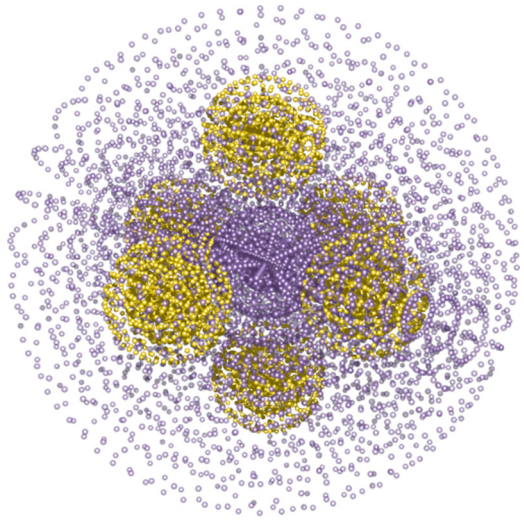

FIG. 1. Schematic representation of an overset grid for calculations on the SF_6 molecule. The actual central and subgrids are denser and radially adaptive.

we have recently introduced an "overset-grid" implementation of the complex Kohn method [18] for electron-molecule scattering making use of a grid-based discrete variable representation of the continuum wave function that replaces its expansion in the analytic basis functions of the earlier implementations. Here we also describe the further extension of that approach to photoionization, and its application to F K-edge ionization in SF_6, which is out of reach of the previous complex Kohn coupled-channel approach and at the limits of the iterative Schwinger variational approach using single center expansions [19,20] for single-channel calculations with which we also compare.

Photoionization calculations on larger systems without local exchange or correlation approximations require both a numerical representation of the continuum components of the wave function and a way to operate with exchange potentials and exchange coupling operators. The overset-grid implementation of the complex Kohn method [18] provides both of those attributes by effectively expanding the scattering wave function simultaneously about multiple centers, as indicated in Fig. 1. As explained in Sec. II, to extend this approach to photoionization we must overcome the fact that it is based on repeated applications of the free-particle Green's function and does not naturally apply Coulomb boundary conditions.

In the following section and in the Appendixes we briefly summarize the complex Kohn variational method and the extension of its overset-grid implementation to photoionization, and provide a benchmark example. In Sec. III we demonstrate the breakdown of the single-channel static-exchange approximation for F K-edge ionization of CF_4 using delocalized orbitals and with that example explore the effects of channel coupling with both localized and delocalized core hole calculations. A principal result of this analysis is a way to avoid the necessity of channel coupling in such cases, no matter how many symmetry equivalent atoms the molecule contains. In Sec. IV we present results on both sulfur and fluorine core ionization in SF_6 using the overset-grid approach, and in Sec. V we summarize our principal conclusions.

II. COMPLEX KOHN VARIATIONAL METHOD FOR PHOTOIONIZATION AND ITS EXTENSION TO OVERSET GRIDS

A. Complex Kohn variational formalism

We begin by briefly describing the complex Kohn variational method for electron-molecule and electron-ion collisions, focusing on how the trial function treats the collision physics while avoiding details of the working equations [16–18]. The traditional implementation, originally developed in the late 1980s [21], uses a mixture of Gaussian and continuum analytic basis functions to form the trial wave function. The more recently developed overset-grid implementation avoids the limitations of using Gaussian basis functions to describe the interaction region, but requires an extension to treat photoionization, which we describe for the first time below and in Appendix A.

For single-channel elastic scattering, the Kohn stationary functional for the scattering T matrix, $T^{+\mathrm{S}}_{\mathbf{k}',\mathbf{k}}$, is a functional of the trial functions, $\psi^{(+)t}_{\mathbf{k}}$ and $\psi^{(-)t}_{\mathbf{k}'}$,

$$T^{+\mathrm{S}}_{\mathbf{k}',\mathbf{k}} = T^{+t}_{\mathbf{k}',\mathbf{k}} + (2\pi)^{-\frac{3}{2}}\left\langle \psi^{(-)t}_{\mathbf{k}'}\middle|\hat{H} - E\middle|\psi^{(+)t}_{\mathbf{k}}\right\rangle, \tag{1}$$

where $T^{+t}_{\mathbf{k}',\mathbf{k}}$ specifies the asymptotic form of the trial function, $\psi^{(+)t}_{\mathbf{k}}$. The two T matrices in Eq. (1) are labeled by asymptotic momenta, and the continuum states are $\delta^3(\mathbf{k}' - \mathbf{k})$ normalized. Importantly for our discussion here, this variational expression is related to a similar one for the photoionization amplitude [22] that is discussed in Appendix B. Expanding the wave functions with incoming $(-)$ and outgoing $(+)$ boundary conditions in partial waves as in Ref. [18]

$$\psi^{(\pm)}_{\mathbf{k}}(\mathbf{r}) = \sqrt{\frac{2}{\pi}}\sum_{l,m} i^l \psi^{(\pm)}_{klm}(\mathbf{r}) Y^*_{l,m}(\hat{\mathbf{k}}), \tag{2}$$

where Y_{lm} denotes a spherical harmonic, produces a partial wave version of Eq. (1)

$$T^{+\mathrm{S}}_{k,l',m',l,m} = T^{+t}_{k,l',m',l,m} + \left\langle \psi^{(-)t}_{kl'm'}\middle|\hat{H} - E\middle|\psi^{(+)t}_{klm}\right\rangle, \tag{3}$$

where l and m denote the angular momentum quantum numbers. The basis set implementation of the complex Kohn method expands the wave function in a combination of the Gaussian basis functions of quantum chemistry, φ_i, and Bessel functions,

$$\psi^{(\pm)t}_{klm}(\mathbf{r}) = \sum_i c^{(\pm)}_i \varphi_i(\mathbf{r}) + \frac{1}{kr}\Bigg[\hat{j}_l(kr)Y_{lm}(\hat{\mathbf{r}}) + \sum_{l',m'} T^{\pm t}_{k,l',m',l,m}\tilde{h}^{\pm}_{l'}(kr)Y_{l'm'}(\hat{\mathbf{r}})\Bigg]. \tag{4}$$

In Eq. (4) $\hat{j}_l(kr)$ denotes the regular Riccati-Bessel function, and $\tilde{h}^{\pm}_l(kr) \xrightarrow{r\to\infty} \hat{h}^{\pm}_l(kr)$ is a function regular at the origin that becomes the outgoing Riccati-Hankel function asymptotically. To apply this method to electron ion scattering, and thus to photoionization, the Bessel functions in Eq. (4) are replaced by Coulomb functions $F_l(k, r)$ and $H_l(k, r)$ with the

asymptotic forms given in Eq. (A4) of Appendix A. In either case the variational parameters in the trial function, namely the coefficients, $c_i^{(\pm)}$, and the T-matrix elements, $T^{\pm S}_{k,l',m',l,m}$, are found by solving linear equations and the stationary approximation to the T matrix, $T^{+S}_{\mathbf{k}',\mathbf{k}}$, is constructed from them in a simple matrix expression given in Refs. [16–18,21].

The multichannel version of the trial function is formed by antisymmetrizing the product of continuum functions like that in Eq. (2) and the bound channel eigenfunctions, $\Phi_\Gamma(\mathbf{r}_1 \cdots \mathbf{r}_N)$ describing electronic states of the target molecule or molecular ion,

$$\Psi^{(\pm)t}_{\Gamma_0,\mathbf{k}_{\Gamma_0}} = \mathcal{A}\sum_\Gamma \Phi_\Gamma(\mathbf{r}_1 \cdots \mathbf{r}_N)\psi^{(\pm)}_{\Gamma,\Gamma_0,\mathbf{k}_{\Gamma_0}}(\mathbf{r}_{N+1}) + \sum_\mu d_\mu^{\Gamma_0,\mathbf{k}_{\Gamma_0}}\Theta_\mu(\mathbf{r}_1 \cdots \mathbf{r}_{N+1}), \tag{5}$$

where the unscattered state has the photoelectron with momentum $\mathbf{k}_{\Gamma_0}$ in the field of the target Φ_{Γ_0} and where we have added closed channel and correlating contributions $\Theta_\mu(\mathbf{r}_1 \cdots \mathbf{r}_{N+1})$. The working equations now additionally include the linear variational parameters, $d_\mu^{\Gamma_0,\mathbf{k}_{\Gamma_0}}$, but still retain the same overall form as for the single-channel case [16,17,23].

The fully differential photoionization cross section for a fixed direction of the polarization vector is related to the dipole matrix element between the neutral and electron-ion scattering wave functions via the relation

$$\frac{d^2\sigma^{\Gamma_0}}{d\Omega_{\hat{\mathbf{k}}_{\Gamma_0}} d\Omega_{\hat{\mathbf{n}}}} = \frac{8\pi\omega}{3c}\left|\langle\Psi_0|\hat{\mathbf{n}}\cdot\boldsymbol{\mu}\left|\Psi^{(-)}_{\Gamma_0,\mathbf{k}_{\Gamma_0}}\right\rangle\right|^2, \tag{6}$$

which defines the cross section for linear polarization $\hat{\mathbf{n}}$ and ejected electron momentum $\mathbf{k}_{\Gamma_0}$ leaving the ion in state Γ_0. The complex Kohn scattering calculation produces the final state wave function $\Psi^{(-)S}_{\Gamma_0,\mathbf{k}_{\Gamma_0}}$ in this expression. If the matrix element in Eq. (6) is evaluated with the Kohn trial function using its variationally determined parameters, it is itself a variational approximation to the photoionization amplitude, as pointed out by Orel and Rescigno [22] and further explained in Appendix B.

The overset-grid representation begins by constructing a compact grid basis of products, $\phi_n(r)Y_{lm}(\theta,\phi)$, of spherical harmonics multiplied by radial discrete variable representation (DVR) functions, $\phi_n(r)$, around each atomic center of the molecule. These "subgrids" do not overlap one another, as indicated in the sketch in Fig. 1 of the overset grid. The subgrids are overlapped by a central grid of the same form that oversets them and reaches to the asymptotic region. The key point of the complex Kohn trial function in Eq. (4) is that it explicitly applies the correct outgoing (or incoming) asymptotic boundary conditions, and that property of the trial function is essential to the working equations. The grid representation does not apply those boundary conditions, so we must do it by another means.

The overset-grid trial function ψ^t is constructed by expanding it in a set of functions that are constructed on the grid by operating with the free-particle Green's function, $\hat{G}_0^+$, which here denotes the Green's function for outgoing boundary conditions $\hat{G}_0^+ \equiv (E - \hat{T} + i\epsilon)^{-1}$, where $\hat{T}$ is the kinetic-energy operator. Expanded in that basis, the trial function analogous to that in Eq. (4) is

$$\psi^{(\pm)t}_{klm}(\mathbf{r}) = \phi^0_{klm}(\mathbf{r}) + \sum_{i=1}^N c_i\,\phi^{(\pm)}_{i,klm}(\mathbf{r}), \tag{7}$$

$$\phi^{(\pm)}_{i,klm}(\mathbf{r}) \equiv (\hat{G}_0^\pm \hat{V})^i \phi^0_{klm}(\mathbf{r}), \tag{8}$$

with $\phi^0_{klm}(\mathbf{r}) = \hat{j}_l(kr)Y_{lm}(\theta,\phi)/kr$ being the incoming wave defined on the central grid. Here, for simplicity, we have written the equations for a single channel case where the potential is denoted by V. This form of the trial function imposes the correct boundary conditions, when the potential does not behave asymptotically as a Coulomb potential, because *all* the functions in the expansion of the trial wave function, except for ϕ^0, satisfy outgoing wave boundary conditions ($\phi^{(+)}_{i,klm}$) or incoming wave boundary conditions ($\phi^{(-)}_{i,klm}$) due to the asymptotic form of $\hat{G}_0^\pm$. However, in the present study we are considering the problem of scattering from an ion, which *does* have a long-range Coulomb potential, for which $\hat{G}_0^\pm$ does not have the correct asymptotic form. In the next section we will discuss how we apply this approach to the problem where the interaction has a Coulomb tail.

The numerical properties of the overset-grid implementation are explored at length in Ref. [18]. In particular, it is shown there that using the iterative basis given in Eq. (7) in the complex Kohn variational expression leads to a sequence of scattering T matrices, where for each N the computed T matrix is equivalent to a $[(N-1)/N]$ Padé approximant to the scattered portion of the T matrix. Maintaining that property, which leads to particularly advantageous numerical properties, in the present application is essential.

B. Extension of the overset-grid implementation to photoionization

A key idea of the overset-grid approach is that the continuum portion of the scattering wave function is expanded in partial waves *simultaneously* about the centers of the central grid and of all the subgrids. This expansion is dramatically more compact than a single-center expansion in spherical harmonics, particularly for larger molecules. To apply scattering boundary conditions we rely on the fact that the result of operating with the free particle Green's function $\hat{G}_0^\pm$ in Eq. (8) produces a function with outgoing (or incoming) boundary conditions. Because $\hat{G}_0^\pm$ is translationally invariant, we can operate with it in the local coordinates of each subgrid, and that is a central simplification that makes the overset-grid approach practical.

The Coulomb Green's function does not have that property so we take another approach. We solve the electron-ion scattering problem truncated at a distance r_0 in the central grid radius at which we can neglect shorter range forces and the Coulomb potential alone dominates the interaction of the continuum electron with the target ion. We can then easily match that solution to the correct Coulomb boundary conditions as described in Appendix A. We have found that more terms in the sum given in Eq. (7) are generally required for convergence with ionic targets than with neutral ones in this procedure, but that the overall computational effort is not

increased by more than about a factor of two over a similar sized neutral problem. In the terminology of Ref. [18], more terms in Eq. (7) are equivalent to more Born-Arnoldi iterations in the solution of the linear equations of the Kohn method.

The static-exchange potential for the scattering of an electron from an ion described by a single configuration which contains one singly occupied orbital has the form

$$V_{\rm SE} = V_{\rm nuc} + \sum_d (2\hat{J}_d - \hat{K}_d) + \hat{J}_s \pm \hat{K}_s, \tag{9}$$

where the sum over d is over doubly occupied orbitals, $\hat{J}$ and $\hat{K}$ are direct and exchange operators, and s refers to the singly occupied orbital for which the sign depends on whether overall singlet or triplet coupling is used for the scattering wave function. The potential $V_{\rm nuc}$ is the nuclear attraction potential. In the special case of a closed shell target (for which the operators defined by the singly occupied orbital are absent), and if the orbitals are Hartree-Fock orbitals, the continuum solution of the Schrödinger equation with this potential is automatically orthogonal to the occupied orbitals. That result derives from the fact that the occupied orbitals are eigenfunctions of the same (Fock) operator as the continuum orbital. However, in all open shell cases orthogonality of the continuum solution to the doubly occupied orbitals is not automatic and must be explicitly enforced. In the basis-set Kohn implementation of electron ion scattering the trial function is made orthogonal to doubly occupied orbitals by construction.

In the extension of the overset-grid approach to photoionization, the needed orthogonality constraint can be applied by a change in the definition of the potential. Applying the constraint that the scattered orbital be orthogonal to the doubly occupied orbitals in that manner retains the Padé property of the Kohn variational expression for the T matrix that underlies its rapid convergence with respect to the number of terms in Eq. (7). The procedure and its working equations are explained in Appendix C.

C. Numerical tests of the overset-grid implementation for photoionization

Although it is much more slowly convergent with respect to partial waves, the iterative Schwinger variational method based on a single center expansion [19,20] can be systematically improved, and so we first compare the overset-grid results for the test case of CF_4 with that approach. Figure 2 compares the integral cross sections and β parameters for ionization of the carbon $1s$ level in the static-exchange approximation from a converged overset-grid calculation with the results of the Schwinger single-center expansion calculation using various numbers of partial waves. The calculation using the overset grid, whose central grid consists of concentric spherical shells of DVR functions, has been converged with respect to the DVR functions, and has a maximum angular momentum of $l = 30$, while the subgrids centered on fluorines have a maximum angular momentum of $l = 3$. The central grid component of the overset grid consists of 42 finite elements (FEM) in a box of 19 Å, in which DVR radial functions are expressed in terms of Legendre polynomials of degree 11 (462 grid points in total). Similarly, each subgrid has 18

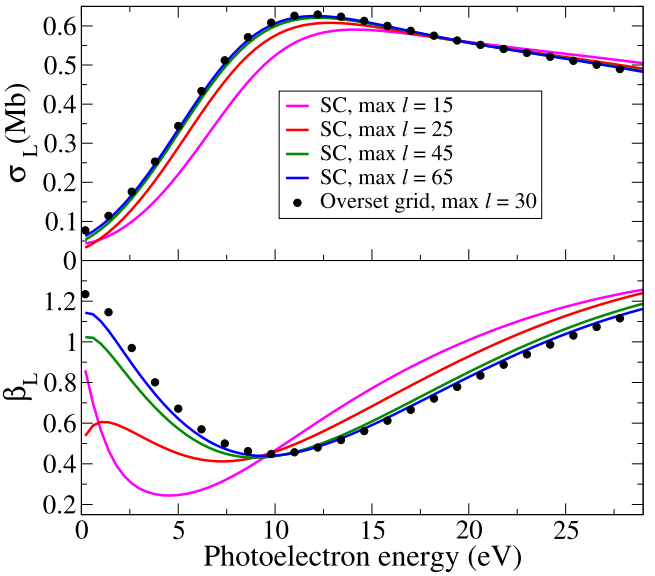

FIG. 2. Integral cross section (top) and β parameter (bottom) for the angular distribution of the photoelectron relative to polarization direction for ionization of the carbon $1s$ orbital in CF_4, comparing the converged overset-grid results with those using the single-center expansion Schwinger iterative method.

FEM in a box of 0.6 Å, which is a distance that insures that the subgrids do not overlap with each other. The underlying DVR quadrature is the same as the central grid, that leads to a total of 198 grid points for each subgrid. The single center expansion results converge towards the overset-grid values as the number of partial waves is increased, verifying the convergence of the overset-grid algorithm for photoionization to the correct result.

In Fig. 3 we compare the results of a basis-set Kohn calculation with those of the overset-grid calculation for the integral cross section for C($1s$) ionization in CF_4. The

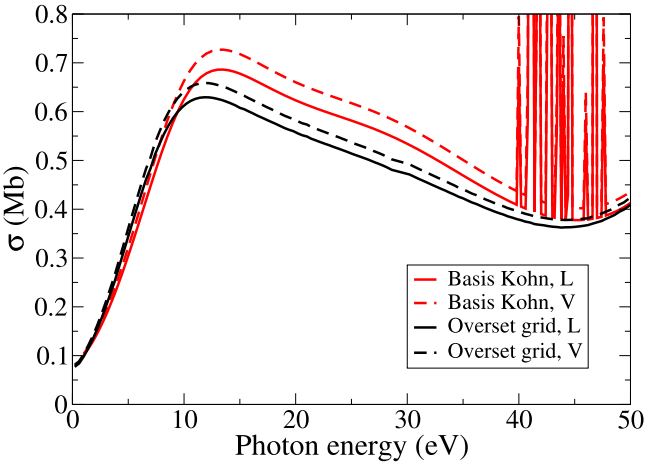

FIG. 3. Integral cross section for C($1s$) ionization in CF_4 comparing basis-set Kohn variational calculations in both length (L) and velocity (V) gauges with converged overset-grid results. The breakdown seen in the basis-set Kohn calculations at energies above 40 eV is due to the limited basis set used in the expansion in Eq. (4).

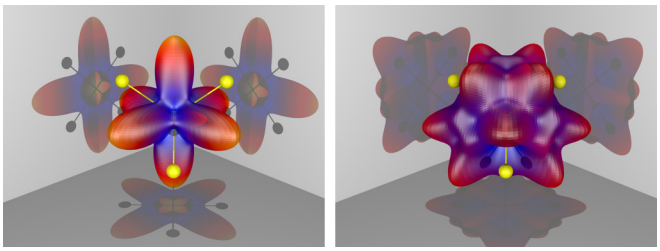

FIG. 4. PA-MFPADs for carbon 1s ionization of CF_4 at 4 eV (left) and 13 eV (right scaled by 2.3). The "anti-imaging" angular dependence on the left is essentially identical to the basis-set Kohn result in Fig. 5 of Ref. [8], where it is compared with experiment.

basis-set Kohn calculations used a maximum of $l = 6$ in trial function in Eq. (4) and a triple-zeta with polarization basis set [24,25] with three additional s-type Gaussians, with exponents 0.08, 0.04, and 0.02, and two p-type Gaussians, with exponents 0.05 and 0.01, at the center of the molecule, for a total of 109 contracted Gaussian basis functions. The differences between the converged overset-grid and basis-set Kohn results for kinetic energies below about 40 eV are primarily the result of inadequacies of the Gaussian basis used in Eq. (4). Also small contributions from higher partial waves are neglected in the basis-set calculations, which would require high angular momentum basis functions not found in typical quantum chemistry packages. However, the spurious features in the basis-set Kohn results at higher kinetic energies are more serious, and likely arise because combinations of the Gaussian functions that would be coupled to higher angular momenta, were they present in the calculation, are partially decoupled from the continuum and thus appear as spurious resonancelike features. On the other hand, the overset grid can be improved systematically by increasing the density of radial DVR functions as well as the number of angular momenta used in the subgrids and central grid so that the overset-grid calculations can be easily extended to kinetic energies of hundreds of eV.

While there are some differences between the overset-grid and basis-set Kohn results for integral cross sections, differences in the angular distributions seen in the computed MFPADs are hardly visible. In Fig. 4 we show polarization averaged MFPADs (PA-MFPADs) for carbon ionization. It is the average over polarization directions that frequently shows the "imaging" behavior or "anti-imaging" (in which electrons appear ejected between the bonds) that have been studied previously [6–9]. These figures are essentially identical to those produced by the basis-set Kohn calculation, differing only slightly in overall magnitude.

Finally we compare MFPADs at a photoelectron energy of 3.0 eV with a fixed polarization direction from overset-grid and basis-set complex Kohn single-channel calculations in the top and middle panels of Fig. 5 at the F K edge to produce an F(1s) hole localized on one of the fluorines. Again there are minimal differences at this energy. However, as one considers lower energies near the Cooper minimum, shown in the basis-set complex Kohn and overset grid integral cross section in Fig. 6, the computed MFPADs are sensitive to the value of the photoelectron energy relative to the location of the Cooper minima in the two calculations. However, when the MFPADs

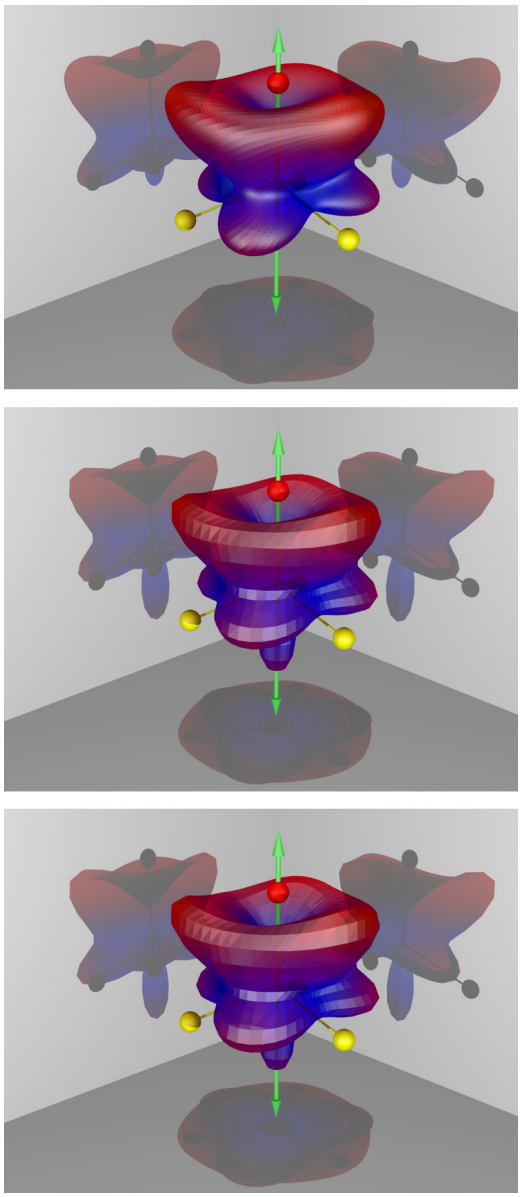

FIG. 5. MFPADs of CF_4 for a 3 eV photoelectron from ionization by linear polarization along a CF bond (two-headed green arrow) for the creation of F(1s) hole localized on the F atom on the polarization axis, which is shown in red. All three calculations used the localized orbitals with one orbital corresponding to the localized F(1s) hole state and the other three F(1s) orbitals being delocalized on the other F atoms. The top panel shows the results from the single-channel overset-grid calculation. The middle panel shows the results from the single-channel basis-set Kohn calculation and the bottom panel shows the basis-set Kohn results with all four F(1s) ionization channels coupled.

at the respective minima, as shown in Fig. 7 for a different polarization direction and without averaging, are compared we again see very good agreement between the overset-grid and basis-set complex Kohn methods.

From the results shown in Fig. 2, with the single-center result converging to the overset-grid result, we are convinced that the overset-grid result is well converged. We have not attempted to converge the basis-set Kohn calculation with

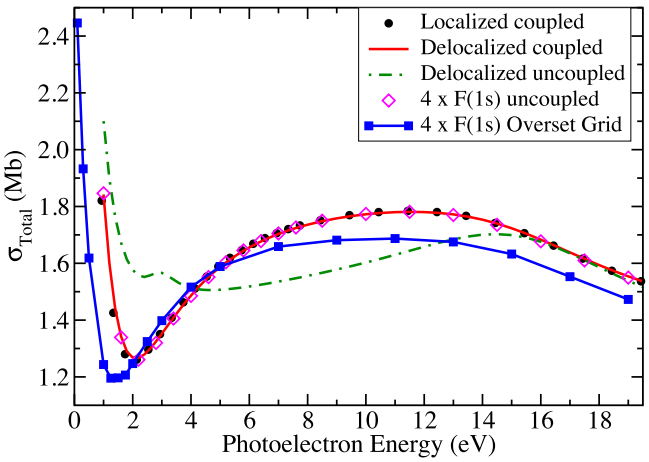

FIG. 6. Total cross sections for F K-edge photoionization in CF_4 from basis-set Kohn calculations in the length gauge summed over the four channels. Curves labeled delocalized have channels defined as vacancies in the four orbitals of a_1 and t_2 symmetry in tetrahedral symmetry. Curves labeled "localized" have one channel defined as a F(1s) vacancy and the other three as vacancies in the remaining a_1 and e symmetry in C_{3v} symmetry. The curves labeled "F(1s)" are four times the cross section for a single channel defined as a vacancy in one fluorine 1s orbital. The overset-grid result for the F(1s) channel is also shown.

respect to the size of the basis, so that of the overset-grid results are most likely the most accurate single-channel static-exchange results given here.

III. USE OF LOCALIZATION TO IMPROVE THE SINGLE-CHANNEL STATIC-EXCHANGE APPROXIMATION FOR CORE IONIZATION

To explore the validity of the single-channel static-exchange approximation for core ionization we first compare the results of several calculations on F K-edge ionization of CF_4. In a Hartree-Fock calculation on the neutral molecule at its equilibrium tetrahedral geometry, the F 1s orbitals form four effectively degenerate molecular orbitals: one a_1 and three t_2 orbitals. If the electronic states of CF_4^+ are defined as single configurations in which an electron is removed from a Hartree-Fock spin orbital, those orbitals define the static-exchange potentials for four single-channel photoionization calculations or the four channels of a coupled channel treatment. We can see the answer to the question of whether channel coupling is important with this definition of the channels in Fig. 6, where the results of such calculations using the basis-set Kohn method are plotted. The coupled channel result is labeled "Delocalized coupled" in that figure. Comparing with the result from the single-channel calculations labeled "Delocalized uncoupled" shows the first effect of making the static-exchange approximation with uncoupled channels. The total cross sections for ionization summed over the four channels differ substantially at low energies, and the Cooper minimum essentially disappears in the uncoupled approximation.

In an earlier study on the observation of the localization of the F(1s) hole we performed calculations with one orbital defined as a F 1s orbital, and the other three transforming with the a_1 and e irreducible representations of the resulting C_{3v} symmetry. Such calculations can be done simply by performing a unitary transformation on the orbitals in T_d symmetry or by very slightly displacing one CF bond distance and allowing the Hartree-Fock calculation to converge to a localized 1s orbital for one of the core molecular orbitals. If the photoionization cross section is calculated with the four resulting channels coupled, the result for the total cross section is the same as if the close-coupling calculation is performed with the orbitals from tetrahedral symmetry, as the points labeled "Localized coupled" in Fig. 6 show.

Also shown in Fig. 6 is the result of multiplying the single channel result for the channel defined as a vacancy in a single F 1s orbital by four. It is essentially identical to the total cross section computed with the four channels coupled for either definition of the channels. Even more striking is the fact that the resulting MFPAD for the F(1s) channel from this single-channel calculation, shown in Fig. 5, is essentially identical to the result for that channel from a four-channel

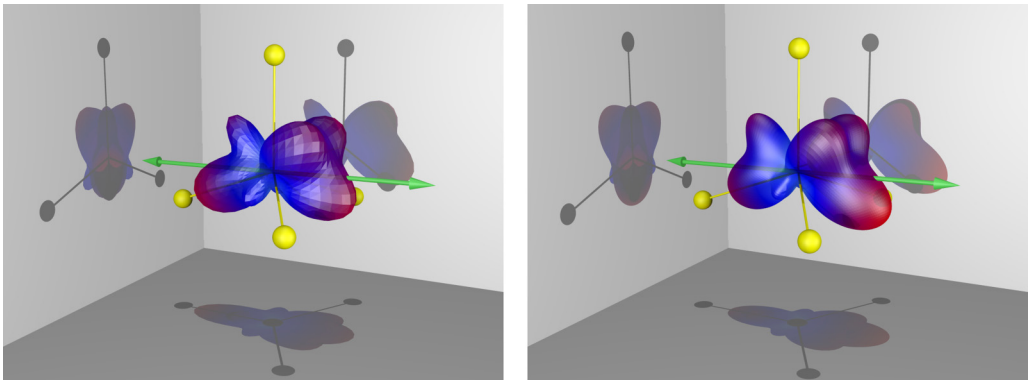

FIG. 7. Comparison of calculated MFPADs for F(1s) ionization of CF_4 by linearly polarized light, with the polarization direction indicated by the two headed green arrows. On the left, the results of a basis-set complex Kohn method at its Cooper minimum (2.18 eV), from a coupled four channel calculation with the MFPAD summed over all four channels. On the right, a single channel overset-grid calculation at its Cooper minimum (1.5 eV), where the F(1s) hole is localized on one F atom and the MFPAD is summed over four such single-channel calculations with the F(1s) hole being localized on the different F atoms.

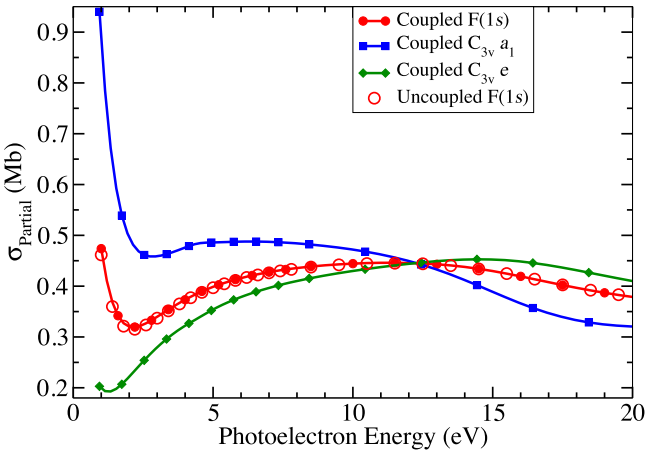

FIG. 8. Partial photoionization cross sections of CF_4 for each of the four channels from coupled-channel basis-set Kohn calculations with one channel defined as a F(1s) vacancy and the other three as vacancies in the remaining C_{3v} symmetry orbitals. The cross sections from the two different e symmetry orbitals are the same. The single-channel (uncoupled) results for the F (1s) hole are shown as symbols alone, and are seen to be nearly identical to the F(1s) coupled channel results.

close coupling calculation. So it appears that localizing that vacancy essentially eliminated that channel's coupling to the other three.

To make sense of this result and to understand its general significance, we examine the contributions of the four channels to the total cross section for coupled-channel calculations with one hole localized on a single fluorine. In Fig. 8 we show the cross sections of the four resulting channels (with holes in the F 1s, a_1, and e orbitals). The sum of these different cross sections (with the cross section for the hole in the e symmetry core orbital multiplied by two) is shown in Fig. 6, where it is labeled "Localized coupled" and is seen to be the same as the coupled channel calculation using the totally delocalized T_d orbitals. Thus the total cross section in a coupled channel calculation is invariant to the definition of the degenerate channels. Additionally, in Fig. 8 we see that the partial cross sections for ionizing to produce an F(1s) vacancy are virtually identical in both the coupled-channel and single-channel calculations when the F(1s) vacancy is localized on one center.

The symmetry breaking in single channel calculations with degenerate channels is seen strikingly in Fig. 9 which shows PA-MFPADs for F K-edge ionization. When the four channels

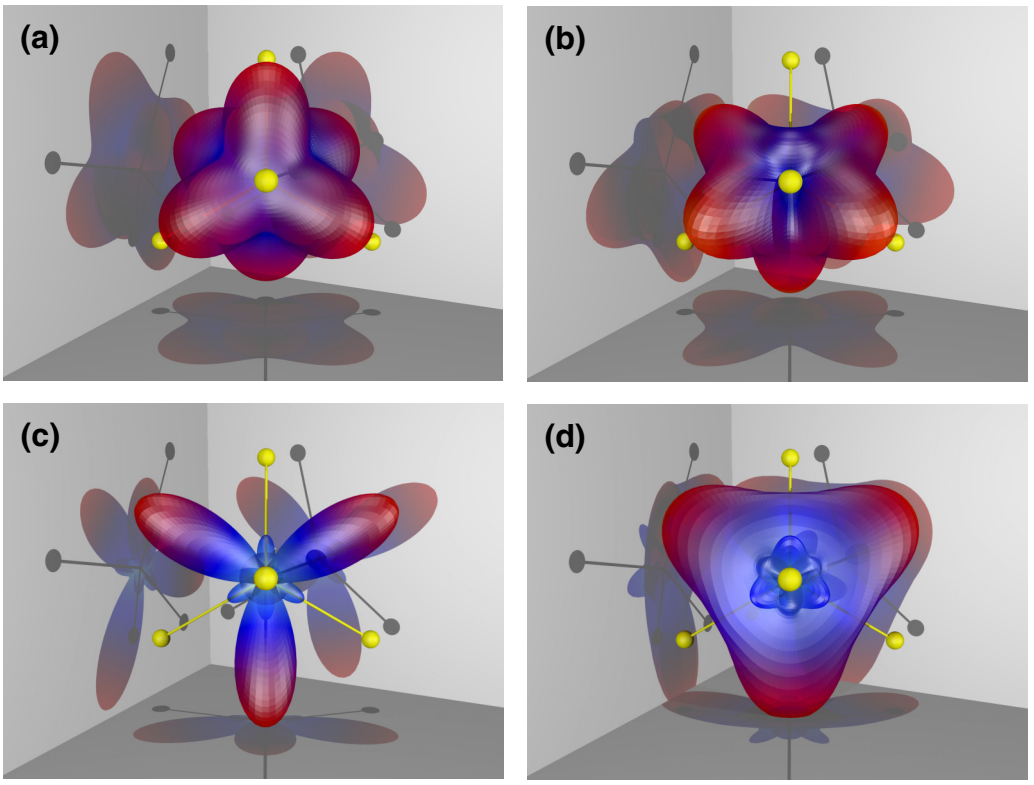

FIG. 9. Calculated PA-MFPADs from delocalized and localized hole states for ionization from the F K-edge in CF_4 2 eV above threshold. (a) The total PA-MFPAD summed over all four channels (a_1 and t_2 orbitals) in tetrahedral symmetry coupling the four channels using delocalized hole states, (b) the same calculation using delocalized hole states with the four channels uncoupled, showing broken symmetry from the single-channel treatment, (c) the same calculation (from the overset-grid implementation) in the full T_d symmetry using delocalized hole states, recovering the symmetry but not the correct coupled channel result, and (d) the PA-MFPAD (times 2.75) for ionization of the localized F(1s) hole on the F atom pointing towards the viewer from the single-channel calculation, which when rotated onto the other three CF directions and summed reproduces (a).

are defined as vacancies in a_1 and t_2 orbitals in tetrahedral symmetry, and used in a close-coupling calculation, the resulting PA-MFPAD reflects the tetrahedral symmetry of the molecule, as it must. However, when the *same channels* are uncoupled using only the C_{2v} point group, and the four single-channel results are summed, the broken symmetry is evident. However, we also show in Fig. 9(c) the results of single-channel calculations, using the overset-grid method, where the full T_d point group is employed. This calculation displays the correct T_d symmetry in the PA-MFPAD, although not the correct result. In particular, we note that the single-channel T_d result has four large lobes in the direction of the C_3 symmetry axes of the molecule opposite to the location of the F atoms on those axes, whereas the correct coupled-channel result shown in Fig. 9(a) has six lobes along the three C_2 axes that bisect the F-C-F bond angles. In the single-channel T_d symmetry calculations, the couplings between the three components of the t_2 orbital are included through the use of symmetry; however, the coupling between the a_1 and t_2 hole states is still neglected.

Nonetheless, if single-channel calculations are performed for ionization from localized F 1*s* orbitals on the four fluorines separately, the resulting PA-MFPADs, one of which is shown in Fig. 9(d), can be added together to recover the correct coupled channels result shown in Fig. 9(a). Defining the channels using the four ion states formed from localized F 1*s* orbitals thus effectively eliminates the coupling between them.

To see why that is the case we can write the operator $\hat{H} - E$ in the coupled channel version of Eq. (1), specializing for clarity to the case of single configuration channel eigenfunctions

$$\hat{\mathbf{H}} - E = \left[\hat{T} - E + V_{\rm nuc} + \sum_o (2\hat{J}_o - \hat{K}_o)\right]\mathbf{1} + \hat{\mathbf{V}}^{\rm CC}, \quad (10)$$

where o is summed over all of the doubly occupied orbitals in the initial state. The form of the channel coupling potential between single configuration hole states is then [3]

$$\hat{V}^{\rm CC}_{i,j} = -\hat{J}_{i,j} + 2\hat{K}_{i,j}, \quad (11)$$

where the coupling operator $\hat{V}^{\rm CC}_{i,j}$ between channel i, with only one electron in orbital φ_i, and channel j, with only one electron in orbital φ_i, operating on the continuum function $\psi_{\mathbf{k}}(\mathbf{r}_1)$ has the form

$$\hat{V}^{\rm CC}_{i,j}\,\psi_{\mathbf{k}}(\mathbf{r}_1) = -\int \frac{\varphi_i^*(\mathbf{r}_2)\varphi_j(\mathbf{r}_2)}{r_{12}} d\mathbf{r}_2\,\psi_{\mathbf{k}}(\mathbf{r}_1) + 2\int \frac{\varphi_i^*(\mathbf{r}_2)\psi_{\mathbf{k}}(\mathbf{r}_2)}{r_{12}} d\mathbf{r}_2\,\varphi_j(\mathbf{r}_1). \quad (12)$$

A unitary transformation among the four orbitals obviously leaves the diagonal first term in $\hat{\mathbf{H}} - E$, defined in Eq. (10), unchanged. Transforming the matrix of potential operators redefines the channels, but cannot break the symmetry of the coupled-channels equations, because the potential matrix has the symmetry of the molecule. That is why the total cross section and PA-MFPADs remain unchanged by such a redefinition of the channels. On the other hand, neglecting all the off-diagonal coupling potentials $\hat{V}^{\rm CC}_{i,j}$, as is done in the single-channel calculations, and making such a transformation on the orbitals produces a diagonal matrix of static exchange potentials that need not reflect the symmetry of the molecule. Two holes might be localized and the other two appear in linear combinations of the remaining two F 1*s* orbitals, for example, with no compensating redefinition of the couplings. This observation explains the symmetry breaking in single-channel calculations in the case of ionization from degenerate core levels.

The result of making the specific unitary transformation that localizes all four of the F 1*s* orbitals, and then neglecting the coupling between those channels, can be seen from the definition of the coupling potential. If the two orbitals φ_i and φ_j are 1*s* orbitals on different fluorines their product is effectively zero and so the first term in Eq. (12) coming from the $\hat{J}_{ij}$ operators, the direct coupling, vanishes. The matrix elements of the exchange coupling, the second term in Eq. (12), are minimized because the products of these two nonoverlaping core orbitals with continuum functions in their respective channels produces two distributions that are strictly localized on the atoms, and which are separated by the distance between the atoms. In contrast, when the hole states are delocalized there will be strong interchannel coupling coming from significant nonzero off-diagonal $\hat{J}_{ij}$ terms.

Thus the separated, single-channel approximation for channels defined in terms of localized orbitals constructed from degenerate core levels is expected to be better than for other choices of channel definitions. Our results here suggest that this choice is in general a very good approximation. Most interestingly, the results of a coupled channel calculation that defines the channels as delocalized symmetry orbitals can be retrieved from the single-channel calculations by transforming the electron-ion scattering T-matrix or photoionization amplitudes back to the symmetry orbital definition of the channels. That fact will make it possible to perform calculations of core photoionization on larger molecules with many equivalent atoms as single-channel static-exchange calculations, but only with the channels defined as localized vacancies.

IV. CORE IONIZATION IN SF_6

For the case of the SF_6 molecule, the close coupling calculations with the basis-set Kohn is out of range, because for the F(1*s*) holes, whether localized or in symmetry orbitals, prohibitively large Gaussian basis sets are required to produce unitary results. Thus, while the basis-set Kohn implementation can treat sulfur core ionization in this molecule, close coupling calculations with that method would be prohibitive for fluorine core ionization.

Nevertheless, the overset-grid implementation does not have this problem with producing unitary results, given the fact that the radial basis is expressed in terms of DVR functions. Therefore, it can be used on this molecule with localized F(1*s*) vacancies defining the channels, and then treating them in single-channel calculations.

For the sake of consistency, we first explore 1*s* and 2*s* ionization of the sulfur atom to demonstrate the convergence properties of the overset-grid implementation, for which other theoretical results have been previously reported [9,20]. First we note that the ionization potential of the S 1*s* orbital is 2490 eV [26]. Thus the wavelength of the light needed to

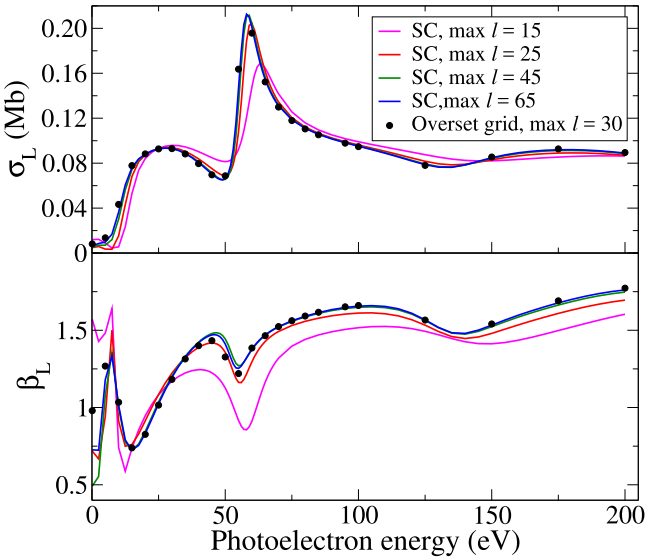

FIG. 10. Photoionization cross section (top) and β parameter (bottom) of SF_6 from the S($1s$) orbital, computed with the single center expansion for different values of the maximum angular momentum ℓ and the converged overset-grid result.

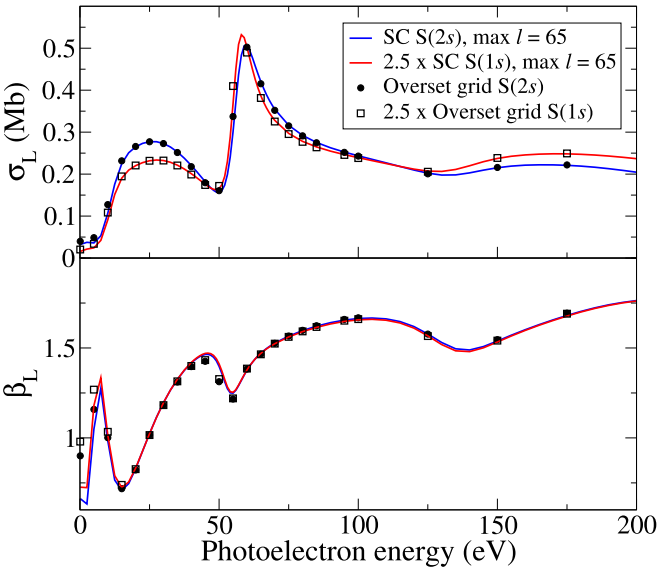

FIG. 11. Comparison of the photoionization of SF_6 from the S($1s$) and S($2s$) orbitals, for the cross section (top) and β parameter (bottom). The cross section corresponding to the S($1s$) photoionization has been resized by a factor of 2.5 to compare better the energy dependence.

ionize from this orbital is $\lambda \leqslant 4.98$ Å, which is on the order of the bond length R(S-F) = 1.561 Å, so that one might expect significant nonzero nondipole effects. However, computed nondipole parameters have shown that these effects are only a few percent of the dipole-allowed parameters [27]. Thus the present results for the dipole MFPAD should be quite close to the MFPADs one would obtain if nondipole effects were included. In Fig. 10, the total photoionization cross section and the β asymmetry parameter, both in the length gauge, are shown for the S($1s$) photoionization. Several results computed with the single-center expansion for several maximum angular momenta $\ell = 15, 25, 45, 65$ clearly point to convergence to the actual result, computed with the overset grid using a moderate value of maximum ℓ. In a similar way that we did for CF_4 in previous sections, a maximum angular momentum $\ell = 30$ for the central grid and $\ell = 3$ for the subgrids located at the fluorine atoms were enough in order to converge the overset-grid calculations with respect to the angular basis. The central grid is expanded in a 7.7 Å spherical box, which is divided in 88 FEM with 440 grid points in total; meanwhile, each subgrid is enclosed in a 0.7 Å box with 170 grid points distributed in 34 FEM. The degree of the underlying Legendre polynomials is 11.

A comparison between the photoionization from the S($1s$) and S($2s$) orbitals is shown in Fig. 11. First we note that the magnitudes of the cross sections are different, with the S($1s$) cross section being approximately 2.5 time smaller than the S($2s$) cross section, which is presumably due to the fact that the S($1s$) core has a much smaller radial extent than the S($2s$) orbital. However, the shapes of the two cross sections are very similar. Both show nearly the same shape resonance around 55 eV in photoelectron energy, which is due to the adiabatic potential corresponding to a partial wave of $\ell = 9$ (see [20] for more details). The β parameters are almost identical, which indicates that the differential cross sections will also differ roughly by the ratio of the total cross sections. The fact that the β parameters are nearly the same was also found by Toffoli *et al.* [27]. We note that in an atomic system the expected value of β for ionization from an s orbital, excluding relativistic effects and assuming that other shells of degenerate atomic orbitals are fully occupied, is $\beta = 2$ [28]. Thus all of the structure seen in the β parameters in Fig. 11 must be due to scattering of the photoelectron by the other parts of the molecule. The fact that the $(1s)^{-1}$ and $(2s)^{-1}$ photoelectron asymmetry parameters are so similar indicates that scattering of the photoelectron by the framework of F atoms must be nearly the same in these two cases.

Considering the static-exchange calculation for the S($2s$), Fig. 12 shows several MFPADs corresponding to different energies around the 55 eV shape resonance for a fixed polarization direction along the main molecular axis. These MFPADs would be almost the same as the S($1s$) MFPADs at the same photoelectron energies, but with a different normalization factor. For energies well below the resonance, the photoelectron also has a high probability to be emitted in several directions other than the polarization one. But, when the energy increases and goes through the resonance, the angular distribution changes dramatically to being strongly peaked along the polarization direction consistent with the high, $l = 7$, decay channel for the shape resonance in this system [20].

In order to describe the photoionization from the F K edge in SF_6, we stretched one of the S-F bonds slightly from equilibrium, resulting in one molecular orbital that consists exclusively of the $1s$ orbital on that fluorine and five others, degenerate and delocalized. This modification of the molecular structure changes the point group symmetry from O_h to C_{4v}, and summing the results of six such calculations, given that in each calculation the hole is located in a different fluorine

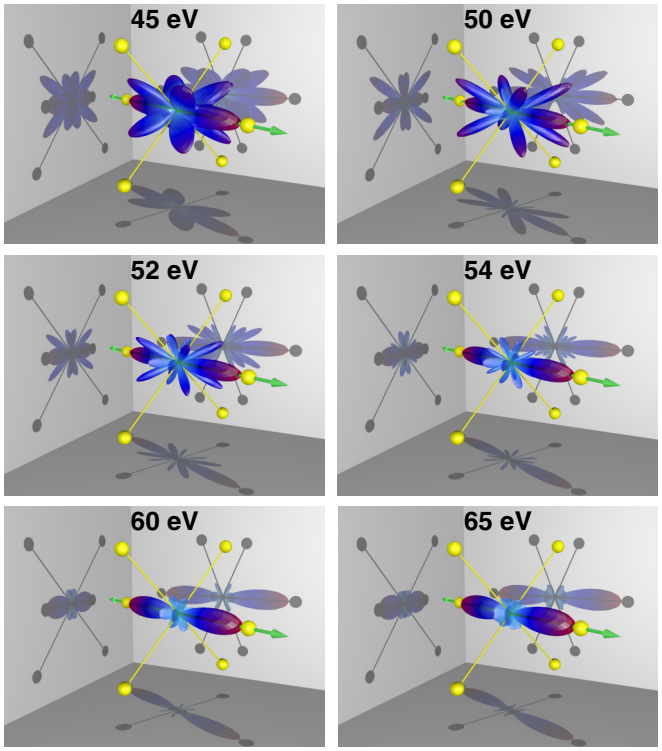

FIG. 12. Calculated MFPADs corresponding to different photoelectron energies (shown in the insets), for the SF_6 photoionization from the S(2*s*) orbital, with a linearly polarized field along one of the main molecule axes.

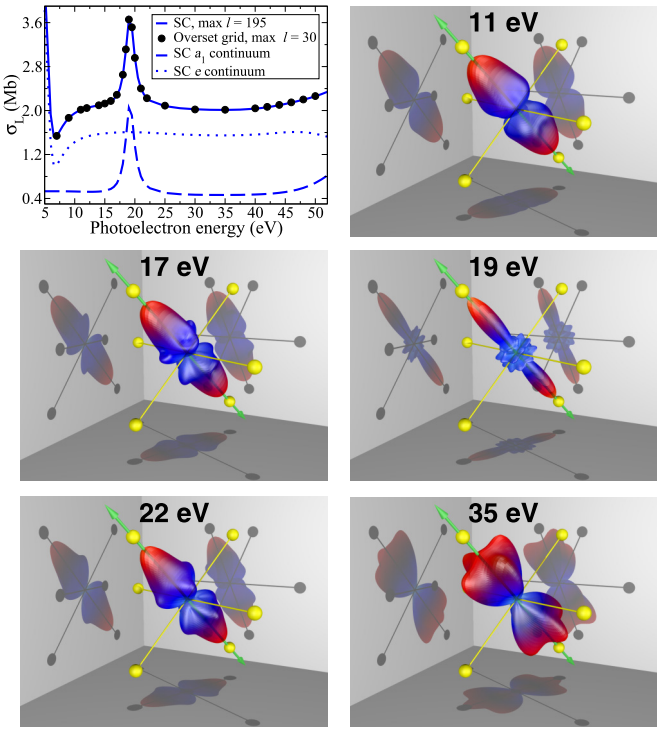

FIG. 13. Total MFPADs corresponding to a fixed polarization direction along the principal molecular axis, for several photoelectron energies (shown in insets) around the shape resonance peak displayed on the top-left panel, obtained adding up the 6 SF_6 photoionization channels that leave the parent ion with a localized 1*s* hole on each fluorine atom.

atom (either stretching the different bonds or properly rotating the matrix elements), produces the result to be expected if no core-hole localization is observed, as shown previously for CF_4. The total cross section and several MFPADs for a fixed polarization along the main molecular axis are shown in Fig. 13. The cross section computed with the single-center Schwinger method required a very high maximum angular momentum $\ell = 195$ in order to converge the result to the one computed with the overset grid. Dividing the cross section into the two photoelectron continuum components, it is clear that the resonance around 19 eV is due to the a_1 component, whilst the e component only contributes as a flat background at energies near the resonance. In addition to the resonance shown in Fig. 13, we find at least two additional shape resonances in the F(1*s*) ionization—one at 55 eV in the a_1 symmetry, which is very similar to the resonance seen in the 1*s* and 2*s* ionization of S seen above, and a resonance at 5 eV in the e continuum. Analyzed in terms of a Fano resonance line shape [29], the cross section of the resonance at 19 eV has a large $q \approx 60$ with a large background cross section that is not coupled to the resonance. In such a situation, one expects that the transition amplitudes will be symmetric about the peak in the cross section. This symmetry is seen in Fig. 13 with the MFPADs corresponding to 17 eV and 22 eV, which are nearly symmetrically displaced from the peak in the cross section which occurs at 19.2 eV. The ionization along the polarization direction is enhanced at the resonant energy indicative of the shape of the MFPAD due to the resonance, whereas away from the resonance, e.g., at 35 eV, broader MFPADs are found.

V. SUMMARY

Our results show that photoionization coupled-channel calculations, with channels defined using delocalized symmetry orbitals for equivalent core holes in the parent ions, can be reproduced with a single-channel calculation by transforming the degenerate delocalized orbitals into localized equivalent hole states. This transformation makes the coupling between different channels almost negligible. This observation would suggest that the model with localized hole states for a system with symmetry equivalent atoms provides the best zeroth-order picture for core ionization in these systems. The approach proposed here for core photoionization calculations is related to the one-center nonorthogonal configuration interaction with single substitutions (1C-NOCIS) method which has been proposed for the study of metastable core-excited states [30]. In the NOCIS method, nonorthogonal configurations based on localized orbitals provide a superior reference basis in which to describe electron correlation in an isolated molecule, while here such configurations provide a better reference from which to describe channel coupling in the presence of the photoelectron, which is also an electron correlation effect. The one center version for core excitation, 1C-NOCIS, limits the configuration interaction wave function to include a single core-hole state much as our one-channel localized hole photoionization calculations only include a single core hole state.

The extension of the overset-grid approach to photoionization, together with the approach to core ionization of

equivalent atoms that allows it to be treated in single-channel calculations, have proven to be successful, and can be used in combination with momentum imaging experiments to explore the question of core-hole localization in larger symmetric molecules such as hexafluorobenzene (C_6F_6) and the other symmetric fluorinated benzenes. Extension of the idea of using localized core holes to simplify core ionization calculations is currently being pursued for the Cl $2p$ ionization of CCl_4, for which experimental recoil frame angular distributions have been measured [31] in a manner similar to the measurements that revealed core hole localization in CF_4 [10]. For core ionization of symmetry nonequivalent atoms, the Hartree-Fock orbitals are naturally localized on those atoms and the single-channel static-exchange approximation should also be sufficient.

The localization of core holes in a core ionization calculation is presented here as a better choice for the ion-state basis set because it minimizes the coupling matrix elements between the different ionization channels. At geometries where the atoms are symmetry equivalent, the canonical Hartree-Fock orbitals are in general delocalized over the symmetry equivalent atoms. When constructing single-configuration ion state wave functions, by removing an electron from one of the initial state orbitals, the Hamiltonian matrix elements between the different resulting $(N-1)$-electron ion states are equal to the matrix elements of the Fock operator between orbitals from which the electrons have been removed. In the case of the canonical Hartree-Fock orbitals all such off-diagonal matrix elements are zero. In contrast, when a unitary transformation is performed on the orbital basis to obtain localized orbitals, the resulting ion states are now connected by nonzero Hamiltonian matrix elements due to the fact that the Fock operator is not diagonal in the new set of orbitals. Note that the Hamiltonian matrix elements between the different localized ion states are proportional to the orbital energy splitting of the delocalized canonical orbitals from which the localized orbitals are constructed. Thus, in the absence of the photoelectron, localizing the hole states induces nonzero Hamiltonian matrix elements between the ion states, although those matrix elements will be small if the canonical orbitals that are being mixed are nearly degenerate. Thus the utility of the core-hole localization approach is based on two facts—the small Hamiltonian matrix elements between the localized ion states and the dramatic reduction of the continuum-continuum interchannel coupling. These two effects are also essential prerequisites to the observation in the photoionization of systems with weakly interacting equivalent core holes, where the lifetime with respect to asymmetric fragmentation is short compared to the hole-hopping time, that the hole does appear to be initially localized at one site, e.g., in the case of $(1s)^{-1}$ ionization of Ne dimer [32,33].

ACKNOWLEDGMENTS

Calculations presented here made use of the resources of the National Energy Research Scientific Computing Center (NERSC), a US Department of Energy Office of Science User Facility operated under Contract No. DE-AC02-05CH11231, and the Lawrencium computational cluster resource provided by the IT Division at the Lawrence Berkeley National Laboratory. Work at LBNL was performed with the support of the US Department of Energy (DOE) under Contract No. DE-AC02-05CH11231. Work at the University of California, Davis was supported by the US Army Research Laboratory and the US Army Research Office under Grant No. W911NF-14-1-0383. C.S.T. was supported in part by a Berkeley Lab Undergraduate Faculty Fellowship (BLUFF). Work performed by L.G. at Kansas State University was supported by the Chemical Sciences, Geosciences, and Biosciences Division, Office of Basic Energy Sciences, Office of Science, U.S. Department of Energy, Grant No. DE-SC0019451.

APPENDIX A: MATCHING TO COULOMB BOUNDARY CONDITIONS

To construct the photoionization amplitude in Eq. (6)

$$A(\mathbf{k}) = \langle \Psi_0 | \hat{\mathbf{n}} \cdot \boldsymbol{\mu} | \Psi_{\mathbf{k}}^{(-)} \rangle, \tag{A1}$$

written here for a single channel for simplicity, we require the partial wave expansion of $\Psi_{\mathbf{k}}^{(-)}(\mathbf{r})$ with Coulomb boundary conditions. Applying the overset-grid approach for neutrals [18] unchanged, we effectively solve for $\Psi_{\mathbf{k}}^{(-)}$ by cutting off the interaction potential at the distance r_0 that marks the limit of the central grid beyond the subgrids and beyond all but the Coulomb potential in the interaction of the continuum electron with the ion. We can change those boundary conditions after the fact by matching to Coulomb boundary conditions at r_0. To perform that matching we first note that the electron-ion scattering wave function with Coulomb boundary conditions can be formally expanded in partial waves as

$$\Psi_{\mathbf{k}}^{(-)} = \left(\frac{2}{\pi}\right)^{1/2} \sum_{l,m,l_0,m_0} \frac{i^{l_0} e^{-i\eta_{l_0}}}{kr} \psi_{l,m,l_0,m_0}^{(-)}(r) \times Y_{l,m}(\hat{\mathbf{r}}) Y_{l_0,m_0}^*(\hat{\mathbf{k}}), \tag{A2}$$

with

$$\psi_{l,m,l_0,m_0}^{(-)}(r) \to F_{l_0}(k,r)\delta_{l,l_0}\delta_{m,m_0} + T_{lm,l_0m_0}^{\mathrm{SR}} H_l^{(-)}(k,r), \tag{A3}$$

where $T_{lm,l_0m_0}^{\mathrm{SR}}$ is the T matrix due to the short range potential in $V = V^{\mathrm{SR}} - Z/r$, where Z is the residual charge of the ion (not necessarily equal to one), η_l is the Coulomb phase shift, and l_0, m_0 labels the regular Coulomb function which is the incoming wave in the asymptotic form and the Coulomb functions satisfy

$$F_l(k,r) \to \sin\left(kr + \frac{Z}{k}\ln 2kr - \frac{\pi l}{2} + \eta_l\right),$$
$$H_l^{(-)}(k,r) \to \exp\left[-i\left(kr + \frac{Z}{k}\ln 2kr - \frac{\pi l}{2} + \eta_l\right)\right]. \tag{A4}$$

The dipole matrix element in Eq. (A1) can be written in terms of this single-center expansion of the scattering wave function as

$$A(\mathbf{k}) = \left(\frac{2}{\pi}\right)^{1/2} \sum_{l_0,m_0} i^{l_0} e^{-i\eta_{l_0}} A_{l_0,m_0} Y_{l_0,m_0}^*(\hat{\mathbf{k}}), \tag{A5}$$

with

$$A_{l_0,m_0} \equiv \left\langle \Phi_0 \middle| \hat{\mathbf{n}} \cdot \boldsymbol{\mu} \middle| \sum_{l,m} \frac{\psi_{l,m,l_0,m_0}^{(-)}(r)}{kr} Y_{l,m}(\hat{\mathbf{r}}) \right\rangle. \tag{A6}$$

We can see that photoionization amplitude is determined by the partial wave amplitudes A_{l_0,m_0} corresponding to angular momenta that contribute to the asymptotic part of the electron-ion scattering wave function, which are the "incoming waves" in the asymptotic form in Eq. (A3). That is in general a much smaller number of partial waves than would be necessary in a single-center expansion of the complete electron-ion scattering wave function.

That observation allows us to use the free-particle Green's function in the Born-Arnoldi iterates, $(G_0V)^n$, in Eq. (8) to solve the complex Kohn equations up to radius of the central grid, r_0, where by doing so we will have applied the boundary conditions

$$\tilde{\psi}^{(-)}_{l,m,l_0,m_0}(r_0) = \hat{j}_l(kr_0)\delta_{l,l_0}\delta_{m,m_0} + \tilde{T}_{lm,l_0m_0}\,\hat{h}^{(-)}_l(kr_0) \quad \text{(A7)}$$

at the point r_0, where the tilde on $\tilde{\psi}^{(-)}_{l,m,l_0,m_0}(r_0)$ denotes that this is the wave function solved with short-range boundary conditions at r_0 and the tilde on $\tilde{T}_{lm,l_0m_0}$ indicates the variational T matrix computed using the complex Kohn variational expression for the cutoff potential. Therefore, at r_0 the radial wave functions from such a calculation are combinations of incoming and outgoing Coulomb functions:

$$\tilde{\psi}^{(-)}_{l,m,l_0,m_0}(r_0) = F_l(k,r_0)\,\alpha_{l\,m,l_0\,m_0} + H^{(-)}_l(k,r_0)\,\beta_{l\,m,l_0\,m_0}. \quad \text{(A8)}$$

The matrices α_{l,m,l_0,m_0} and β_{l,m,l_0,m_0} can be calculated simply from matching the value and derivative of the wave function; denoting $\partial/\partial r$ by primes, we first define

$$W_{H^{(-)}_l}(f_l) = \left.\frac{H^{(-)'}_l f_l - f_l' H^{(-)}_l}{H^{(-)'}_l F_l - F_l' H^{(-)}_l}\right|_{r_0} = \left.\frac{-1}{k}\left(H^{(-)'}_l f_l - f_l' H^{(-)}_l\right)\right|_{r_0}, \quad \text{(A9)}$$

where we used the Wronskian of the Coulomb functions. Then using the corresponding expression for F_l, we easily find that

$$\alpha_{lm,l_0m_0} = W_{H^{(-)}_l}(\hat{j}_l)\delta_{l,l_0}\delta_{m,m_0} + \tilde{T}_{lm,l_0m_0}W_{H^{(-)}_l}(\hat{h}^{(-)}_l), \quad \text{(A10)}$$

$$\beta_{lm,l_0m_0} = W_{F_l}(\hat{j}_l)\delta_{l,l_0}\delta_{m,m_0} + \tilde{T}_{lm,l_0m_0}W_{F_l}(\hat{h}^{(-)}_l). \quad \text{(A11)}$$

Note that α_{l,m,l_0,m_0} and β_{l,m,l_0,m_0} are written in terms of two quantities that only depend on the value of r_0 and k and the variational $\tilde{T}$ so that both α and β are variational.

Now if we define the right inverse of the matrix α by

$$\sum_{l',m'} \alpha_{l\,m,l'\,m'}\;\alpha^{-1}_{l'\,m',l_0\,m_0} = \delta_{l,l_0}\delta_{m,m_0}, \quad \text{(A12)}$$

we can transform (rotate) the outgoing waves so that they have Coulomb boundary conditions

$$\sum_{l_0',m_0'} \tilde{\psi}^{(-)}_{l,m,l_0',m_0'}(r_0)\;\alpha^{-1}_{l_0'\,m_0',l_0\,m_0} = F_l(k,r_0)\,\delta_{l,l_0}\delta_{m,m_0} + H^{(-)}_l(k,r_0)\,T^{\rm SR}_{l\,m,l_0\,m_0},$$
$$T^{\rm SR}_{l\,m,l_0\,m_0} \equiv \sum_{l_0',m_0'} \beta_{l\,m,l_0'\,m_0'}\;\alpha^{-1}_{l_0'\,m_0',l_0\,m_0}. \quad \text{(A13)}$$

A similar expression for the photoionization amplitudes can be written in terms of the dipole matrix elements calculated with $\tilde{\psi}$ using cutoff-potential boundary conditions,

$$\tilde{A}_{l_0,m_0} = \left\langle \Phi_0 \middle| \hat{\mathbf{n}}\cdot\boldsymbol{\mu} \middle| \sum_{l,m} \frac{\tilde{\psi}^{(-)}_{l,m,l_0,m_0}(r)}{kr}\,Y_{l,m}(\hat{\mathbf{r}}) \right\rangle \quad \text{(A14)}$$

can be transformed directly using

$$A_{l_0,m_0} = \sum_{l_0',m_0'} \tilde{A}_{l_0',m_0'}(r_0)\;\alpha^{-1}_{l_0'\,m_0',l_0\,m_0}, \quad \text{(A15)}$$

and these transformed amplitudes are the ones that appear in Eq. (A6) for the correct photoionization amplitudes.

APPENDIX B: KOHN VARIATIONAL PRINCIPLE FOR PHOTOIONIZATION AMPLITUDE

From the discussion in Appendix A, we can conclude that a variational estimate of the transition matrix elements A_{l_0,m_0} can be obtained if we can compute the variational $\tilde{T}_{lm,l_0m_0}$ and a variational estimate of the transition moment with the cutoff potential $\tilde{A}_{l_0',m_0'}$. It has been shown [22] that the complex Kohn variational method can be used to compute a transition moment involving a scattering state. In particular, a variational expression for $\tilde{A}(\mathbf{k})$ can be written as

$$\tilde{A}^{\rm S}(\mathbf{k}) = \langle\Psi_0|\hat{\mathbf{n}}\cdot\boldsymbol{\mu}\big|\tilde{\Psi}^{(-)t}_{\mathbf{k}}\rangle + \langle\tilde{f}^{(+)t}|\hat{\mathbf{n}}\cdot\boldsymbol{\mu}\big|\tilde{\Psi}^{(-)t}_{\mathbf{k}}\rangle, \quad \text{(B1)}$$

where $\tilde{\Psi}^{(-)t}$ is a variational trial function to $\tilde{\Psi}^{(-)}$ and $\tilde{f}^{(+)t}$ is a variational trial function for $\tilde{f}^{(+)}$, which is the solution of the equation

$$(\hat{H}-E)|\tilde{f}^{(+)}\rangle + (\hat{\mathbf{n}}\cdot\boldsymbol{\mu})|\Psi_0\rangle = 0. \quad \text{(B2)}$$

Then as long as

$$\tilde{f}^{(+)t} \xrightarrow[r\to\infty]{} \sum_{l'm'} \hat{h}^{(+)}_{l'}(r)Z_{l'm'}Y_{l'm'}(\hat{r}), \quad \text{(B3)}$$

Eq. (B1) is indeed variational.

One can then show that, if $\tilde{\Psi}^{(-)t}_{\mathbf{k}}$ and $\tilde{f}^{(+)t}$ are written as linear variational functions with the same basis functions, the expression in Eq. (B1) can be written as

$$\tilde{A}^{\rm S}(\mathbf{k}) = \langle\Psi_0|\hat{\mathbf{n}}\cdot\boldsymbol{\mu}\big|\tilde{\Psi}^{(-){\rm S}}_{\mathbf{k}}\rangle, \quad \text{(B4)}$$

where $\tilde{\Psi}^{(-){\rm S}}$ is the linear trial function where the expansion coefficients yield a stationary T matrix.

APPENDIX C: ORTHOGONALITY CONSTRAINTS REQUIRED FOR OPEN SHELL TARGETS

A crucial element needed to apply the present photoionization calculation scheme is to enforce the orthogonality between the occupied orbitals of the target $|\phi_i\rangle$ and the electronic scattering states $|\psi^{(-)}_{klm}\rangle$, which we achieve introducing a pseudopotential $\tilde{V}$. Defining the projector operator Q over all the occupied orbitals,

$$Q = \sum_i^n |\phi_i\rangle\langle\phi_i|, \quad \text{(C1)}$$

we restrict the Schrödinger equation for the scattering states to the constrained form

$$(1-Q)(\hat{H}-E)(1-Q)|\psi^{(-)}_{klm}\rangle = 0. \quad \text{(C2)}$$

Developing the left-hand side of (C2) and substituting $\hat{H} = \hat{T} + V$, we end up expressing the constrained Schrödinger equation as

$$(\hat{T} + \tilde{V} - E)|\psi_{klm}^{(-)}\rangle = 0, \tag{C3}$$

where the effective potential $\tilde{V}$, known as a Phillips-Kleinman pseudopotential [34,35], is given by

$$\tilde{V} = V - Q(\hat{H} - E) - (\hat{H} - E)Q + Q(\hat{H} - E)Q. \tag{C4}$$

It is important to notice that the way we have introduced the orthogonality constraints through a modified effective potential $\tilde{V}$ ensures that the Krylov basis defined in Eq. (8) is also orthogonal to the occupied orbitals, without losing the Padé approximant feature of the trial function $\psi_{klm}^{(\pm)t}(\mathbf{r})$ in Eq. (7). Due to the fact that the aforementioned Krylov space basis leads to a solution in a form of Padé approximants (see [18] and the references therein), a fast convergence rate is achieved.

[1] T. N. Rescigno, B. H. Lengsfield III, and A. E. Orel, J. Chem. Phys. **99**, 5097 (1993).
[2] B. Basden and R. R. Lucchese, Phys. Rev. A **34**, 5158 (1986).
[3] B. Basden and R. R. Lucchese, Phys. Rev. A **37**, 89 (1988).
[4] R. R. Lucchese and A. Stolow, J. Phys. B: At. Mol. Opt. Phys. **45**, 190201 (2012).
[5] K. L. Reid, Mol. Phys. **110**, 131 (2012).
[6] J. B. Williams, C. S. Trevisan, M. S. Schöffler, T. Jahnke, I. Bocharova, H. Kim, B. Ulrich, R. Wallauer, F. Sturm, T. N. Rescigno, A. Belkacem, R. Dörner, T. Weber, C. W. McCurdy, and A. L. Landers, Phys. Rev. Lett. **108**, 233002 (2012).
[7] C. S. Trevisan, C. W. McCurdy, and T. N. Rescigno, J. Phys. B: At. Mol. Opt. Phys. **45**, 194002 (2012).
[8] A. Menssen, C. S. Trevisan, M. S. Schöffler, T. Jahnke, I. Bocharova, F. Sturm, N. Gehrken, B. Gaire, H. Gassert, S. Zeller, J. Voigtsberger, A. Kuhlins, F. Trinter, A. Gatton, J. Sartor, D. Reedy, C. Nook, B. Berry, M. Zohrabi, A. Kalinin, I. Ben-Itzhak, A. Belkacem, R. Dörner, T. Weber, A. L. Landers, T. N. Rescigno, C. W. McCurdy, and J. B. Williams, J. Phys. B: At. Mol. Opt. Phys. **49**, 055203 (2016).
[9] E. Plésiat, P. Decleva, and F. Martín, Phys. Rev. A **88**, 063409 (2013).
[10] C. W. McCurdy, T. N. Rescigno, C. S. Trevisan, R. R. Lucchese, B. Gaire, A. Menssen, M. S. Schöffler, A. Gatton, J. Neff, P. M. Stammer, J. Rist, S. Eckart, B. Berry, T. Severt, J. Sartor, A. Moradmand, T. Jahnke, A. L. Landers, J. B. Williams, I. Ben-Itzhak, R. Dörner, A. Belkacem, and T. Weber, Phys. Rev. A **95**, 011401(R) (2017).
[11] R. Guillemin, P. Decleva, M. Stener, C. Bomme, T. Marin, L. Journel, T. Marchenko, R. K. Kushawaha, K. Jänkälä, N. Trcera, K. P. Bowen, D. W. Lindle, M. N. Piancastelli, and M. Simon, Nat. Commun. **6**, 6166 (2015).
[12] R. R. Lucchese, H. Fukuzawa, X.-J. Liu, T. Teranishi, N. Saito, and K. Ueda, J. Phys. B: At. Mol. Opt. Phys. **45**, 194014 (2012).
[13] S. Tsuru, M. Kazama, T. Fujikawa, J. ichi Adachi, T. Mizuno, and A. Yagishita, Chem. Phys. Lett. **608**, 152 (2014).
[14] W. H. Miller and B. M. D. D. Jansen op de Haar, J. Chem. Phys. **86**, 6213 (1987).
[15] C. W. McCurdy, T. N. Rescigno, and B. I. Schneider, Phys. Rev. A **36**, 2061 (1987).
[16] T. N. Rescigno, C. W. McCurdy, A. E. Orel, and B. H. Lengsfield III, in *Computational Methods for Electron-Molecule Collisions* (Springer, New York, 1995), pp. 1–44.
[17] T. N. Rescigno, B. H. Lengsfield III, and C. W. McCurdy, in *Modern Electronic Structure Theory*, edited by D. R. Yarkony (World Scientific, Singapore, 1995), Vol. 1, pp. 501–588.
[18] L. Greenman, R. R. Lucchese, and C. W. McCurdy, Phys. Rev. A **96**, 052706 (2017).
[19] F. A. Gianturco, R. R. Lucchese, and N. Sanna, J. Chem. Phys. **100**, 6464 (1994).
[20] A. P. P. Natalense and R. R. Lucchese, J. Chem. Phys. **111**, 5344 (1999).
[21] C. W. McCurdy and T. N. Rescigno, Phys. Rev. A **39**, 4487 (1989).
[22] A. E. Orel and T. N. Rescigno, Phys. Rev. A **41**, 1695 (1990).
[23] B. H. Lengsfield and T. N. Rescigno, Phys. Rev. A **44**, 2913 (1991).
[24] T. H. Dunning, J. Chem. Phys. **53**, 2823 (1970).
[25] T. H. Dunning and P. J. Hay, in *Methods of Electronic Structure Theory*, edited by H. F. Schaefer, Modern Theoretical Chemistry (Plenum Press, New York, 1977), pp. 1–28.
[26] R. E. LaVilla, J. Chem. Phys. **57**, 899 (1972).
[27] D. Toffoli and P. Decleva, J. Chem. Phys. **128**, 234101 (2008).
[28] S. T. Manson and A. F. Starace, Rev. Mod. Phys. **54**, 389 (1982).
[29] U. Fano, Phys. Rev. **124**, 1866 (1961).
[30] K. J. Oosterbaan, A. F. White, D. Hait, and M. Head-Gordon, Phys. Chem. Chem. Phys. **22**, 8182 (2020).
[31] T. Weber (private communication).
[32] M. Yamazaki, J.-i. Adachi, Y. Kimura, A. Yagishita, M. Stener, P. Decleva, N. Kosugi, H. Iwayama, K. Nagaya, and M. Yao, Phys. Rev. Lett. **101**, 043004 (2008).
[33] K. Kreidi, T. Jahnke, T. Weber, T. Havermeier, R. E. Grisenti, X. Liu, Y. Morisita, S. Schössler, L. P. H. Schmidt, M. Schöffler, M. Odenweller, N. Neumann, L. Foucar, J. Titze, B. Ulrich, F. Sturm, C. Stuck, R. Wallauer, S. Voss, I. Lauter, H. K. Kim, M. Rudloff, H. Fukuzawa, G. Prümper, N. Saito, K. Ueda, A. Czasch, O. Jagutzki, H. Schmidt-Böcking, S. K. Semenov, N. A. Cherepkov, and R. Dörner, J. Phys. B: At. Mol. Opt. Phys. **41**, 101002 (2008).
[34] J. D. Weeks, A. Hazi, and S. A. Rice, in *Advances in Chemical Physics* (John Wiley & Sons, New York, 2007), pp. 283–342.
[35] R. R. Lucchese, G. Raseev, and V. McKoy, Phys. Rev. A **25**, 2572 (1982).